prosthesis

MDPI

Article

Effects of Hysteresis on the Dynamic Deformation of Artificial Polymeric Heart Valve

Shahrul Hisyam Marwan [1] and Mitsugu Todo [2,*]

[1] School of Mechanical Engineering, College of Engineering, Universiti Teknologi MARA (UiTM), Terengganu Branch, Bukit Besi Campus, Dungun 23200, Terengganu, Malaysia
[2] Research Institute for Applied Mechanics, Kyushu University, 6-1 Kasuga-koen, Kasuga 816-8580, Japan
* Correspondence: todo@riam.kyushu-u.ac.jp

Abstract: The deformation behavior of an artificial heart valve was analyzed using the explicit dynamic finite element method. Time variations of the left ventricle and the aortic pressure were considered as the mechanical boundary conditions in order to reproduce the opening and closing movements of the valve under the full cardiac cycle. The valve was assumed to be made from a medical polymer and hence, a hyperelastic Mooney–Rivlin model was assigned as the material model. A simple formula of the damage mechanics was also introduced into the theoretical material model to express the hysteresis response under the unloading state. Effects of the hysteresis on the valve deformation were characterized by the delay of response and the enlargement of displacement. Most importantly, the elastic vibration observed in the pure elastic response under the full close state was dramatically reduced by the conversion of a part of elastic energy to the dissipated energy due to hysteresis.

Keywords: artificial heart valve; explicit finite element method; hyperelastic material; hysteresis; cardiac cycle

Citation: Marwan, S.H.; Todo, M. Effects of Hysteresis on the Dynamic Deformation of Artificial Polymeric Heart Valve. *Prosthesis* **2022**, *4*, 511–523. https://doi.org/10.3390/prosthesis4040042

Academic Editor: Salvatore Pasta

Received: 16 June 2022
Accepted: 18 September 2022
Published: 21 September 2022

1. Introduction

The aortic valve of the heart is one of the most important organs in our body system. The position of the aortic valve is in between the aorta and the left ventricle, which distributes blood to our body system. The aortic valve is made of three moving thin flaps of tissue called cusps or leaflets that come together in the center of the valve to close it [1] and to ensure only one-directional blood flow through the cardiovascular system [2]. Every year, over 100,000 patients in the United States have to go through surgical procedures to replace their malfunctioning heart valves with artificial heart valves [3].

At present, prosthetic heart valves (PHV) have widely been available commercially in the field of cardiac surgery, including mechanical heart valves (MHV) and bio-prosthetic heart valves (BHV). MHVs are usually made from pyrite carbon (artificial carbon), and the performance is relatively durable but patients are likely to get thromboembolic (blood clotting) problems [4]. Therefore, patients who are using MHVs always need to take an anticoagulant drug, which may cause life-threatening hemorrhages if poorly managed [5]. On the other hand, the natural BHVs have excellent hemodynamic properties (no need for anticoagulant drugs) but they are less durable compared with MHVs [5]. The patients who are using BHVs generally need to experience another surgery after 15 to 20 years. Khan et al. conducted a 20-year post-operation follow-up study on 2533 cases of patients aged 18 years or older who had used MHVs or BHVs [6]. Their study exhibited that in general, there were no survival rates for both types of valves, with similar complications. From this perspective, it is concluded that both types of PHVs have still been suffering from several drawbacks, and an ideal PHV with high durability without thrombotic problems has not been developed yet.

In contrast, polymeric valves (PVs) have been investigated and developed as an alternative artificial value that may potentially address the limitations of both BHVs and MHVs. PVs ideally have a similar advantage to BHVs whose leaflets are flexible. Such flexibility can enhance blood flow and improve blood disruption as well as lifelong biostability. One of the most important characteristics of PVs is their high durability. Actually, PVs have been studied since the 1950s [7–11], and in the 1960s, the first PVs were implanted in aortic [7] and human mitral locations [11]. However, based on the clinical outcomes, these initial trials were not successful because the polymers available at the time did not provide sufficient biostability and durability. However, currently, as a result of advanced technology in polymer engineering, excellent biostable polymers that may fulfill the clinical requirements of PVs have extensively been developed. These include a new generation of polytetrafluoroethylene [12], polyurethane urea [13], polyurethane with a poly (dimethylsiloxane) soft segment (Elast-Eon) [14], poly (styrene-b-isobutylene-b-styrene) (SIBS) [15], and Bionate polycarbonate urethane (PCU) [16].

Gharaie and Morsi analyzed an optimized PV design made from Bionate using the fluid structure interaction analysis and concluded that the optimized valve demonstrated high hemodynamic performance with no sign of damaging stress concentration in the entire cardiac cycle. In their analysis, they used the hyperelastic Mooney–Rivlin model for the Bionate valve. However, the experimental study conducted by Ghaill and Little clearly exhibited a viscoelastic mechanical behavior of Bionate, which included a hysteresis response in the stress-strain relation [17]. The Mooney–Rivlin model is a well-known and frequently chosen model because it has a reputation for accurately predicting the reaction of hyperelastic materials [18]. The inclusion of linear dependency in the strain energy function is what causes such improved accuracy. This means that the first and second invariants specify the deviatoric response. Other than that, the third-order approximation of the Mooney–Rivlin model for incompressible systems is well recognized to be more appropriate for describing shear deformations in elastomers [19].

The aim of this study was therefore to develop a three-dimensional finite element (FE) model of the tri-leaflets aortic polymeric valve with a nonlinear hyperelastic model including hysteresis response. The PV was designed on the basis of the optimized design developed by Gharaie and Morsi [7]. The Mooney–Rivlin model was used to express the hyperelastic mechanical response, along with a hysteresis model in which a damage factor was introduced to control the hysteresis response. Dynamic finite element analysis was then performed to examine the open-close response of the PV under a time-dependent pressure condition imitating a full cardiac cycle. Effects of hysteresis on the dynamic deformation during the closing motion were then carefully analyzed.

2. Methods

2.1. Development of 3D FE Model of Artificial Heart Valve

A 3D CAD model of an artificial heart valve was constructed using the computer-aided design software Autodesk Fusion 360 by referring to the substantial details of the geometry given by the earlier work done by Gharaie and Morsi [7]. The external appearances of the 3D model having asymmetric tri-leaflet are shown in Figure 1. The height, diameter, and thickness of the 3D model are 8.5, 25.0, and 0.5 mm, respectively. The 3D CAD model was then exported to the explicit dynamic finite element code LS-DYNA (Liverware Software, Livermore, CA, USA), and then the finite element meshes were created. Eight-node hexahedral elements were used and the numbers of element and node were 5670 and 9036, respectively. It was assumed that the valve was made from an engineering polymer whose mechanical properties are similar to those of biological tissue used for BHVs. Therefore, the Mooney–Rivlin hyperelastic model was used as the material model for the FE model. A hysteresis model was also introduced into the hyperelastic model to express the nonlinear behavior under unloading conditions. The density and the Poisson's ratio were set to be 1190 kg/m^3 [20] and 0.4924 [17], respectively.

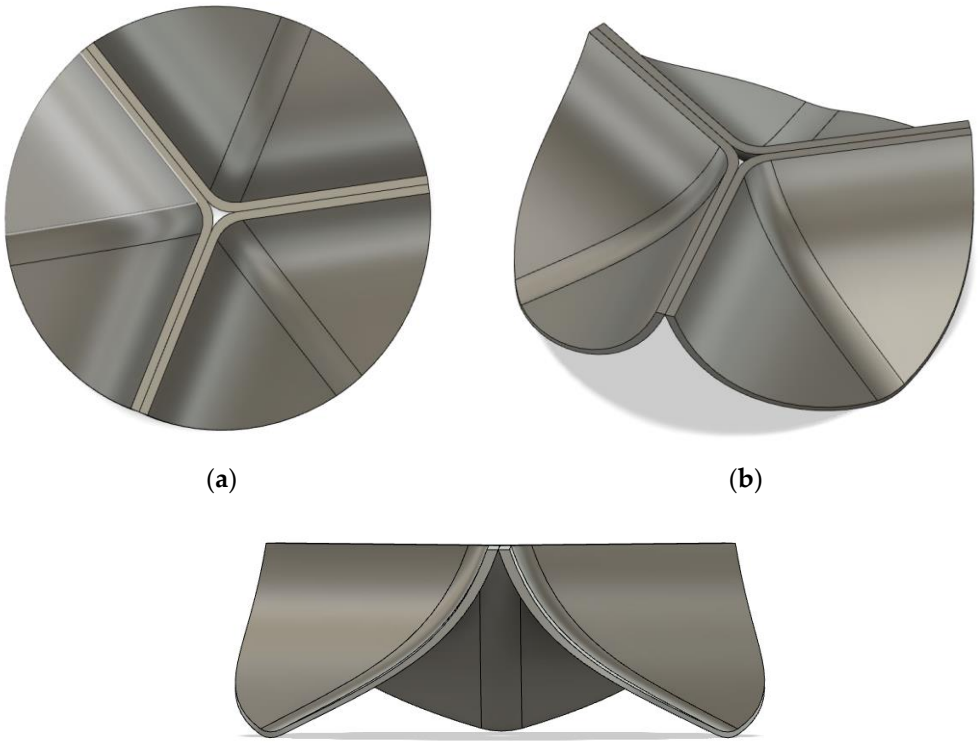

(**a**) (**b**)

(**c**)

Figure 1. External appearances of artificial human heart valve with asymmetric tri-leaflet. (**a**) Top view, (**b**) Isometric view, and (**c**) Side view.

To increase the model's dependability and confidence, 3D FE models must be verified. Additionally, the verification of a 3D FE model of asymmetric tri-leaflets with linear and non-linear material properties was done in this study in order to compare the findings from earlier studies. For the linear material properties, the density, Young's modulus, and Poisson's ratio were set to 1020 kg/m^3 [21], 5.0 MPa [21], and 0.45 [21], respectively. For the non-linear properties, the density and Poisson's ratio were adjusted to 1000 kg/m^3 [20] and 0.495 [17], respectively.

2.2. Hyperelastic Material Model

The strain energy density function of the three-term Mooney–Rivlin model is given by [17]:

$$W = C_{10}(I_1 - 3) + C_{01}(I_2 - 3) + C_{11}(I_1 - 3)(I_2 - 3) \quad (1)$$

where the strain invariants are given by:

$$I_1 = \lambda_1^2 + \lambda_2^2 + \lambda_3^2,\ I_2 = \lambda_1^2\lambda_2^2 + \lambda_2^2\lambda_3^2 + \lambda_3^2\lambda_1^2 \quad (2)$$

as the functions of the principal stretch ratios λ_1 and λ_2. The constitutive equation is then obtained from:

$$\boldsymbol{S} = \frac{\partial W}{\partial \boldsymbol{E}} \quad (3)$$

where $\boldsymbol{S}$ and $\boldsymbol{E}$ are stress and strain tensors, respectively. In the present analysis, the values of C_{10}, C_{01}, and C_{11} were chosen to be -0.55, 1.338, and 0.23 MPa, respectively.

2.3. Hysteresis Model

A typical nonlinear stress-stretch response with hysteresis is illustrated in Figure 2. The loading path is expressed by O-a-b, following the unloading path b-c-O. This inelastic

nonlinear response is called "hysteresis". The area surrounded by the hysteresis loop can be understood as the dissipated energy by microstructural damage formations such as the plastic flow of macromolecules in viscoelastic polymers and rubbers [21,22].

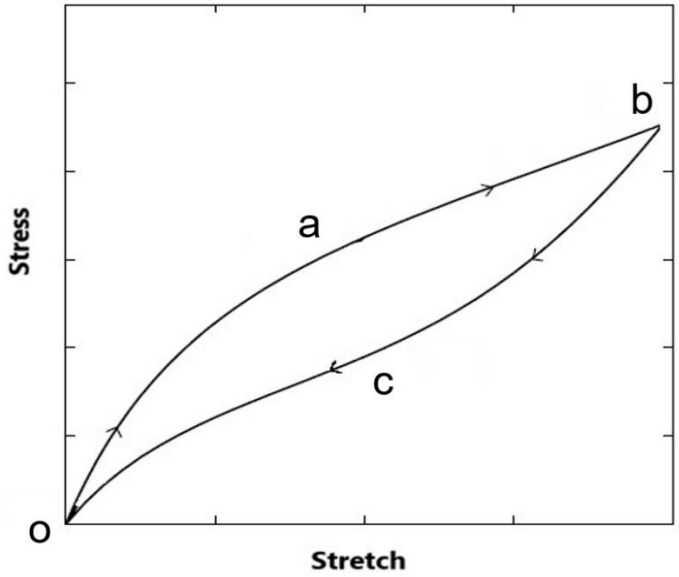

Figure 2. Stress-stretch behavior with hysteresis under simple tension.

Such hysteresis behavior can be expressed theoretically by introducing the damage mechanics. It is assumed that under unloading condition, the constitutive equation can be derived [22]:

$$\boldsymbol{S} = D\frac{\partial W}{\partial \boldsymbol{E}} \tag{4}$$

where D is called the damage factor. It is defined that D varies from 0 at $W = 0$ to 1 at $W = W_{\max}$ where $W = 0$ expresses the original state of deformation (no loading) and $W = W_{\max}$ is equivalent to the maximum strain energy density at the end of the loading state. In the present analysis, D was assumed to be simply expressed as a linear function of W:

$$D = kW, \quad 0 \le W \le W_{\max} \tag{5}$$

$W_{\max}$ was determined from the maximum internal energy of the valve model without hysteresis at the fully opened condition. The constant k can be calculated from the relationship:

$$k = \frac{1}{W_{\max}} \tag{6}$$

Dynamic finite element analysis of simple tensile testing was conducted to examine the effects of the hysteresis model. It was related to the stress-stretch behavior under a loading and unloading condition during the simple tensile testing. In the simple tensile testing, the material of the tensile specimen was assumed to be the same polymer used for the artificial valve. The stress-stretch response is shown in Figure 3. It can be seen that a hysteresis loop was successfully created using the theoretical model described above.

2.4. Boundary Conditions

By considering the real movement of the human aortic valve and in order to obtain smooth opening and closing behavior, all the nodes along the side edges of the asymmetry leaflet were fixed in all directions. Such a geometric boundary condition is shown in Figure 4a.

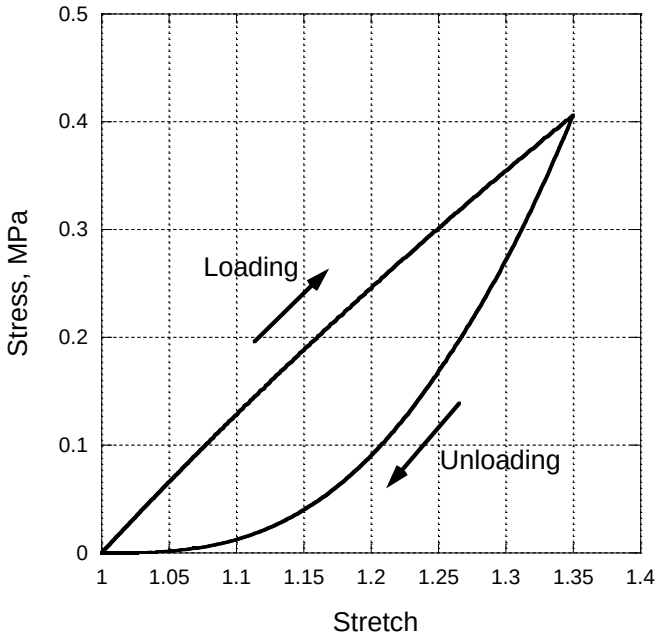

Figure 3. Stress-stretch relations under simple tension with hysteresis.

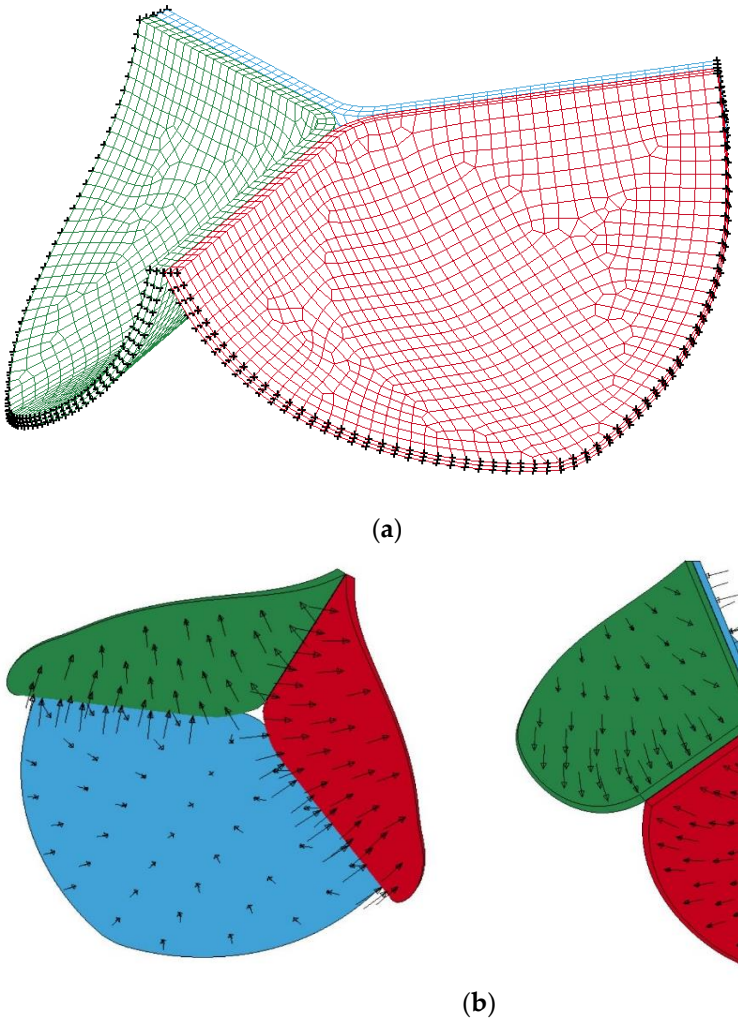

(**a**)

(**b**)

Figure 4. Geometrical and mechanical boundary conditions. (**a**) Geometric boundary condition, and (**b**) Mechanical boundary conditions (**left**: inner layer, **right**: outer layer).

The asymmetry tri-leaflets were constructed with two layers of element for each leaflet. The inner and outer layers were classified as the ventricular and the aortic surface, respectively. Then, the left ventricle and the aortic pressure were assigned to the inner ventricle and the outer aortic surface, respectively, as shown in Figure 4b. The time variations of the left ventricular and the aortic pressure were assumed for one cardiac cycle with a nominal rate of 75 beats/min, and are shown in Figure 5 [7].

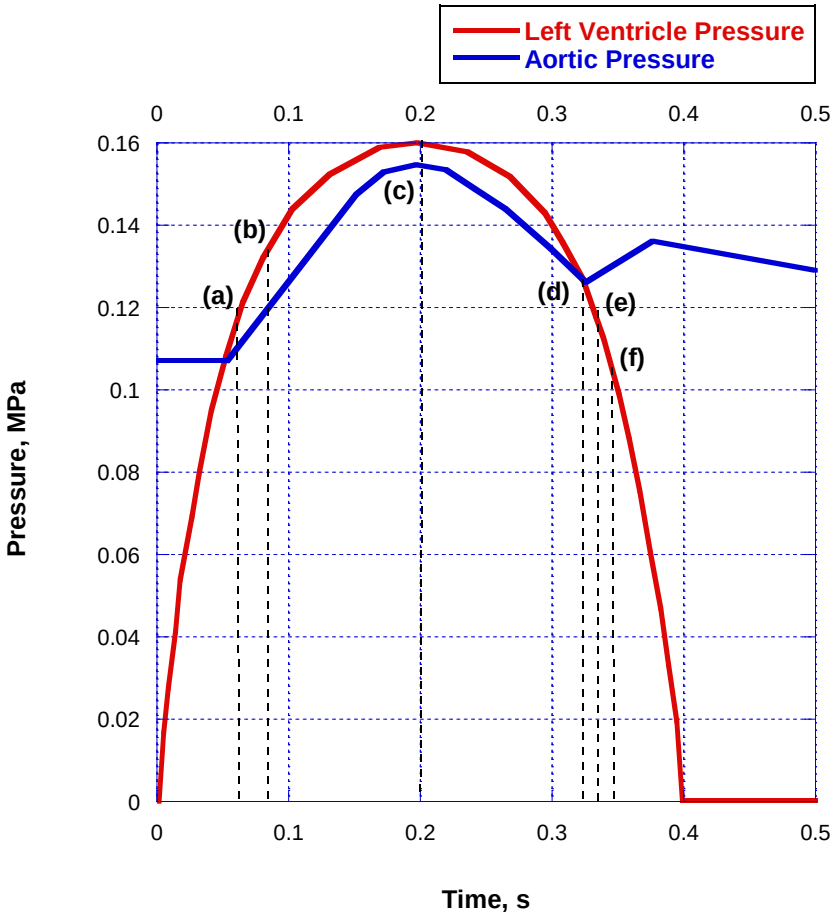

Figure 5. Time-varying pressure loading applied in the FEM simulation over a full cardiac cycle [7].

3. Results and Discussion

3.1. Verification of 3D FE Model of the Asymmetry Tri-Leaflet

The stress on the valve in the cardiac cycle was examined in earlier studies of the linear material properties. According to Ranga A. et al., the top of the attachment line between the leaflets and the aortic root wall, called the commissures, is where the leaflets are discovered to exert the maximum stress on the root wall during diastole, as seen in Figure 6 [23]. In this study, we also observe at the same location to compare the simulation result (Figure 7) with the referenced result as shown in Figure 8 [23]. The value and pattern are not significantly different between these two results, as can be observed. Consequently, the 3D model of the asymmetric tri-leaflets for the linear material model was verified and validated.

The displacement result of the position at the B node was observed in earlier research for the non-linear material properties as shown in Figure 9a, and it was also observed in this study as shown in Figure 9b. A comparison is then made between the study's displacement at node B result, shown in Figure 10, and the reference result, shown in Figure 11. The value and pattern are not significantly different between these two outcomes, as can be observed. As a result, the 3D model of the asymmetric tri-leaflets was verified and validated for the non-linear material model as well.

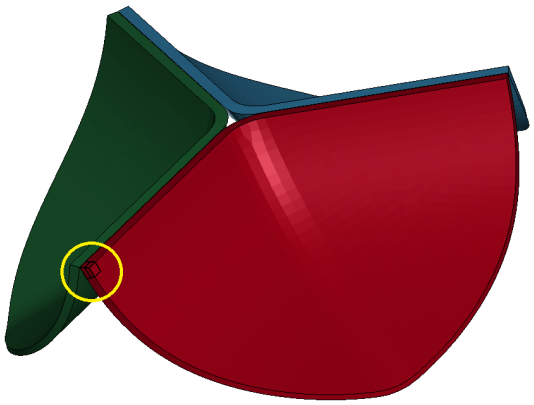

Figure 6. The location of commissure point of the 3D model of asymmetry tri-leaflet.

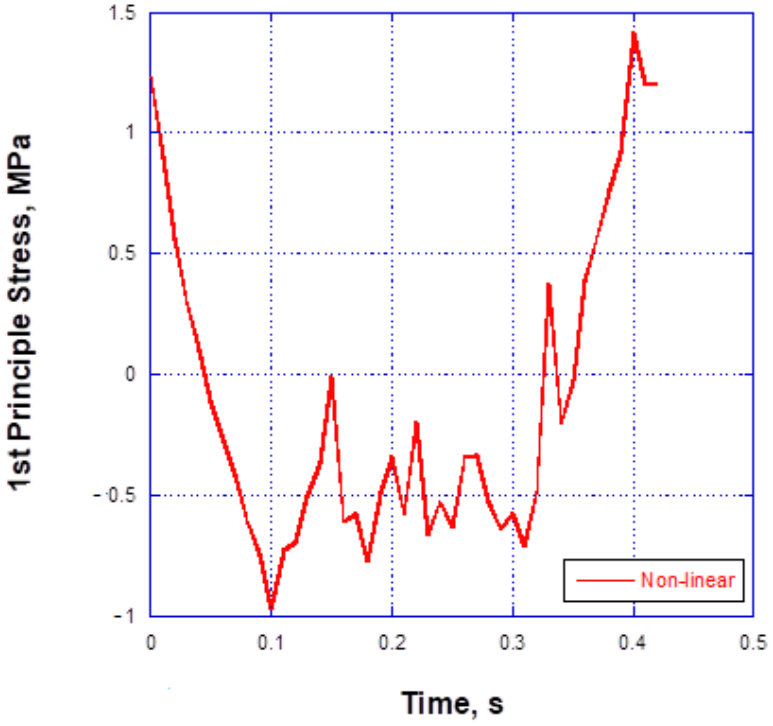

Figure 7. Plot of 1st principal stress vs. time at commissure point in the present study.

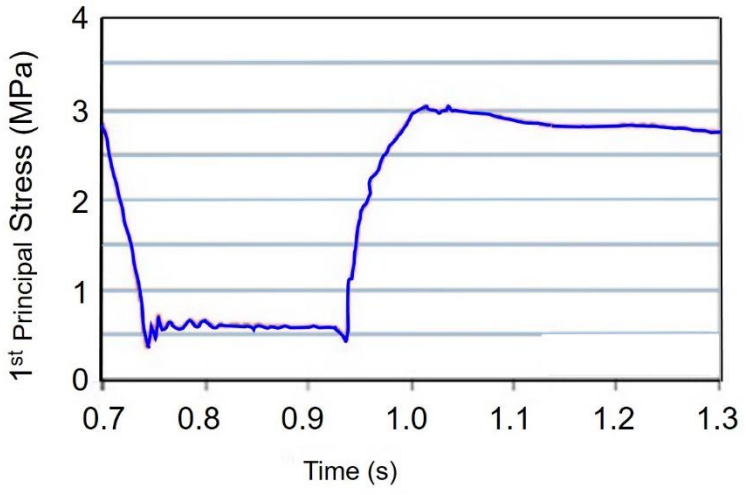

Figure 8. Plot of 1st principal stress vs. time at commissure point [23].

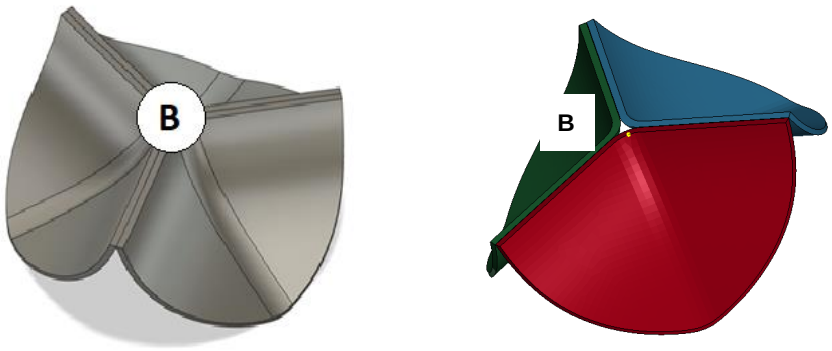

(**a**) (**b**)

Figure 9. The location node B of the 3D model of asymmetry tri-leaflet, (**a**) In previous study [24] (**b**) In the present study.

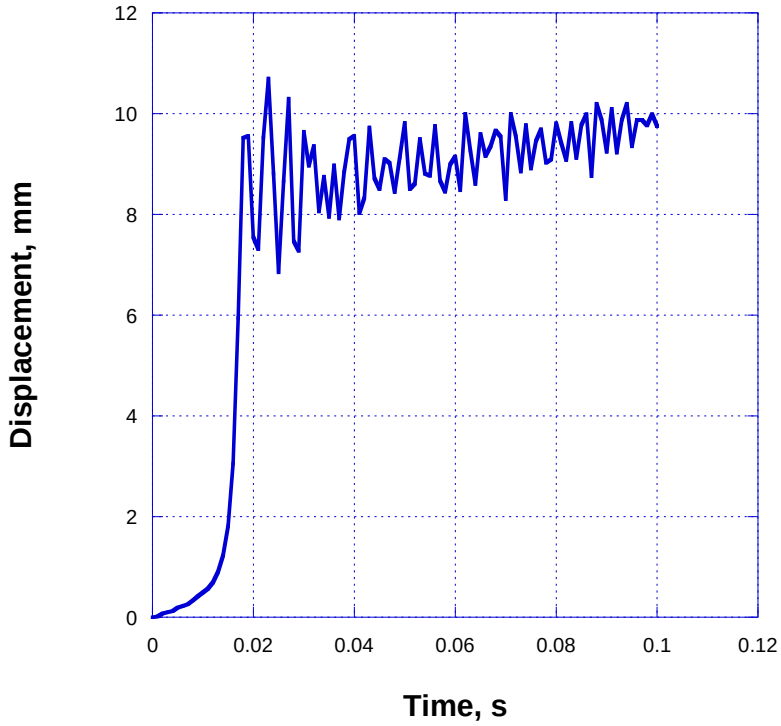

Figure 10. Displacement in characteristic B node in the present study.

3.2. Dynamic Deformation Behavior of the Asymmetry Tri-Leaflet

During the full cardiac cycle in the FE analysis, the tri-leaflet valve started to open just before t = 0.05 s when the left ventricle pressure exceeded the aortic pressure and reached the fully open state at t = 0.08 s (the point (b) in Figure 5). The valve tended to slightly close up to t = 0.32 s (the point (d)). Then, the valve showed rapid closing behavior up to t = 0.34 s (the point (f)). The deformation behaviors of the tri-leaflets were observed at the six points shown in Figure 5. The deformed images observed from the front are shown in Figure 12 without hysteresis and Figure 13 with hysteresis. It can be seen that the deformation behaviors with hysteresis were similar to those without hysteresis during this opening state ((a) and (b)) and slightly closing state ((c) and (d)) with minor hysteresis effect. On the other hand, the deformation behaviors with and without hysteresis were very different at points (e) and (d) under the rapid closing state. Especially, the edges of the leaflets were deformed unnaturally with curved shapes without hysteresis, suggesting that the elastic vibration of the membrane structures took place during the closing condition. Those curved deformations were dramatically reduced with hysteresis. Especially, the leaflets were fully closed along the straight lines at point (f).

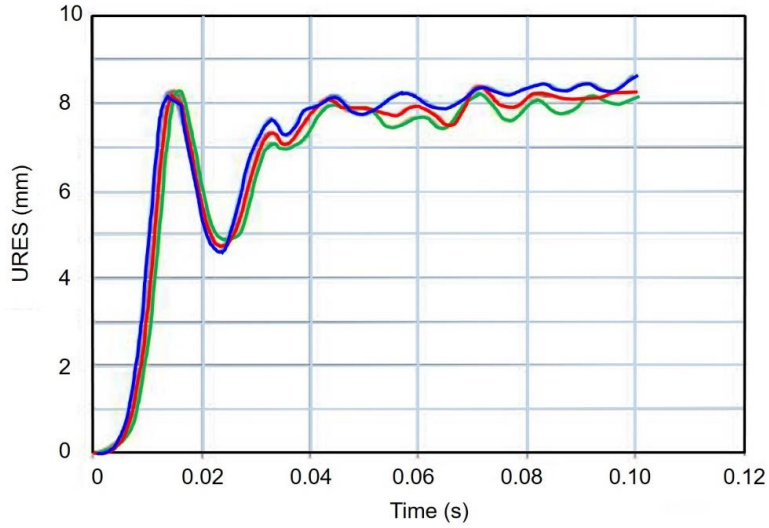

Figure 11. Displacement in characteristic B node [24].

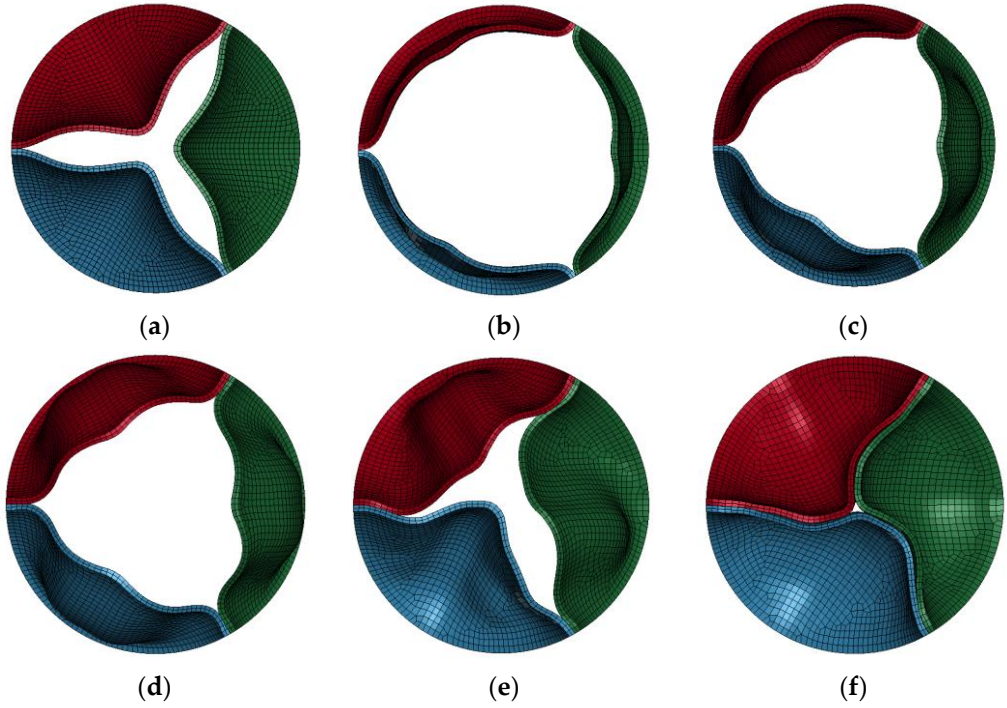

Figure 12. Deformation behaviors of the leaflets without hysteresis. (**a**) t = 0.06 s, (**b**) t = 0.08 s, (**c**) t = 0.2 s, (**d**) t = 0.32 s, (**e**) t = 0.33 s, and (**f**) t = 0.34 s.

3.3. Effects of Hysteresis on Internal Energy and Displacement

Time-dependent behaviors of the internal energy with and without hysteresis are shown in Figure 14. The "internal energy" implies the elastic energy stored in the body without hysteresis, while it corresponds to the sum of the elastic energy and the absorbed energy by damage formation with hysteresis. The internal energy started at 1.29 mJ, which was the elastic energy due to the deformation by the initial constant aortic pressure (see Figure 5). Then, the energy decreased as the left ventricle pressure increased and reached the minimum level (t = 0.04 s) at which the valve fully closed. It is noted that the energy with hysteresis was higher than that without hysteresis at this minimum level, indicating that some amount of energy was absorbed by hysteresis during the unloading condition up to t = 0.05 s. The energy increased from point (a) to (b) (the fully open condition shown in Figures 12b and 13b under the opening state). The energy without hysteresis tended to decrease from point (b) to (d) where the leaflets slightly closed and then rapidly closed

from point (d) to (f). On the contrary, the energy tended to remain almost constant from point (b) to (e) where the elastic energy was thought to decrease due to the slight closing condition, while the dissipated energy by the hysteresis tended to increase.

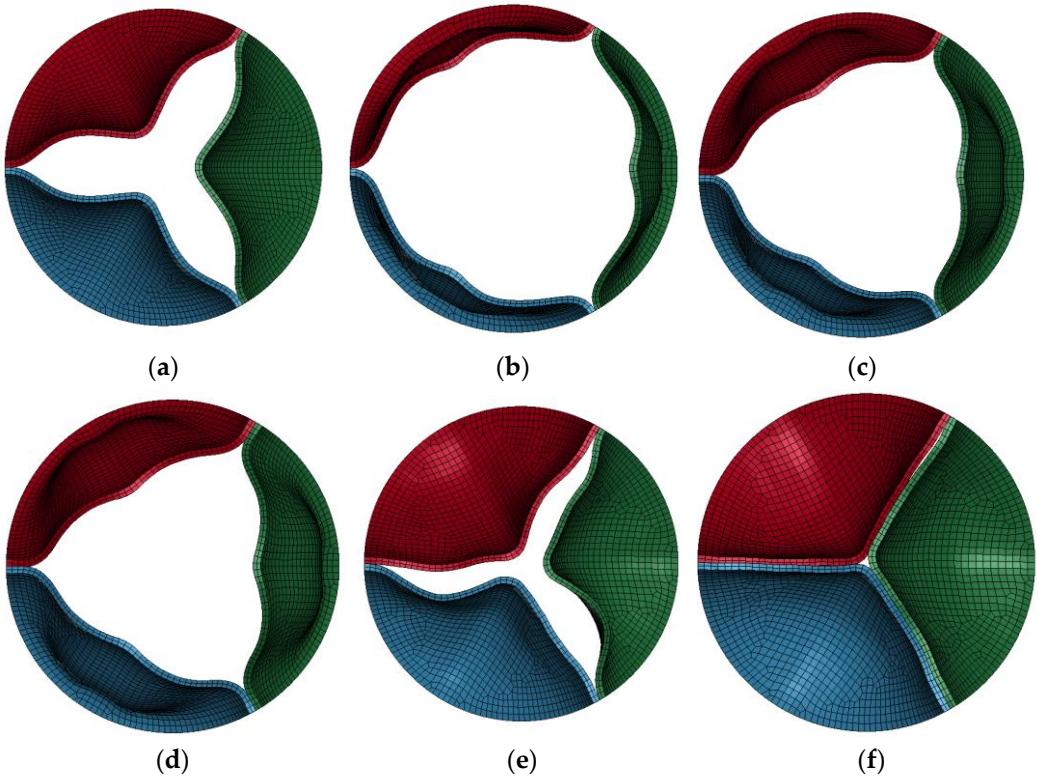

Figure 13. Deformation behaviors of the leaflets with hysteresis. (**a**) t = 0.06 s, (**b**) t = 0.08 s, (**c**) t = 0.2 s, (**d**) t = 0.32 s, (**e**) t = 0.33 s, and (**f**) t = 0.34 s.

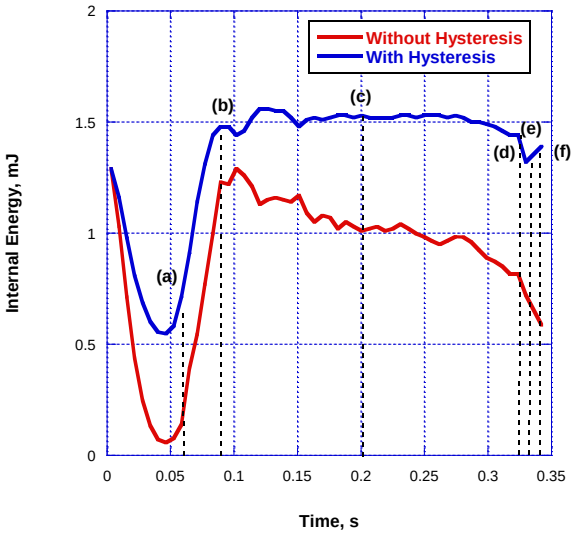

Figure 14. The stored energy of the leaflet with hysteresis and without hysteresis vs. time.

The time variations of displacement were also evaluated at the three points A, B, and C shown in Figure 15. The measured displacements are shown in Figure 16. The displacements at points A and C well expressed the opening state (t = 0.05 to 0.1 s), the slight closing state (t = 0.1 to 0.32 s), and the rapid closing state (t = 0.32 to 0.34 s), while the displacement at the point B was very different from A and C because B is located close to the fixed edge. By comparing those graphs with and without hysteresis, the effects of hysteresis on the displacements have two characteristics: one is the delay during the

opening state as seen from t = 0.05 to 0.1 s and another is the enlargement observed from t = 0.2 to 0.32 s.

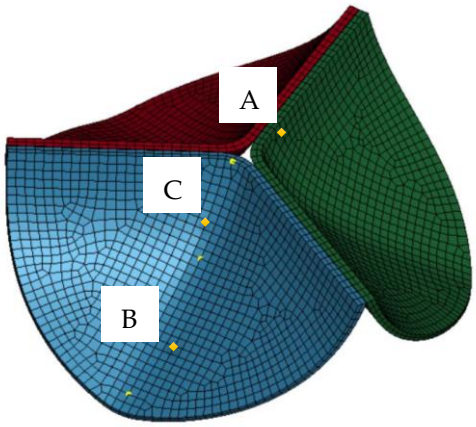

Figure 15. The location of node A, B, and C of the 3D model of asymmetry tri-leaflet.

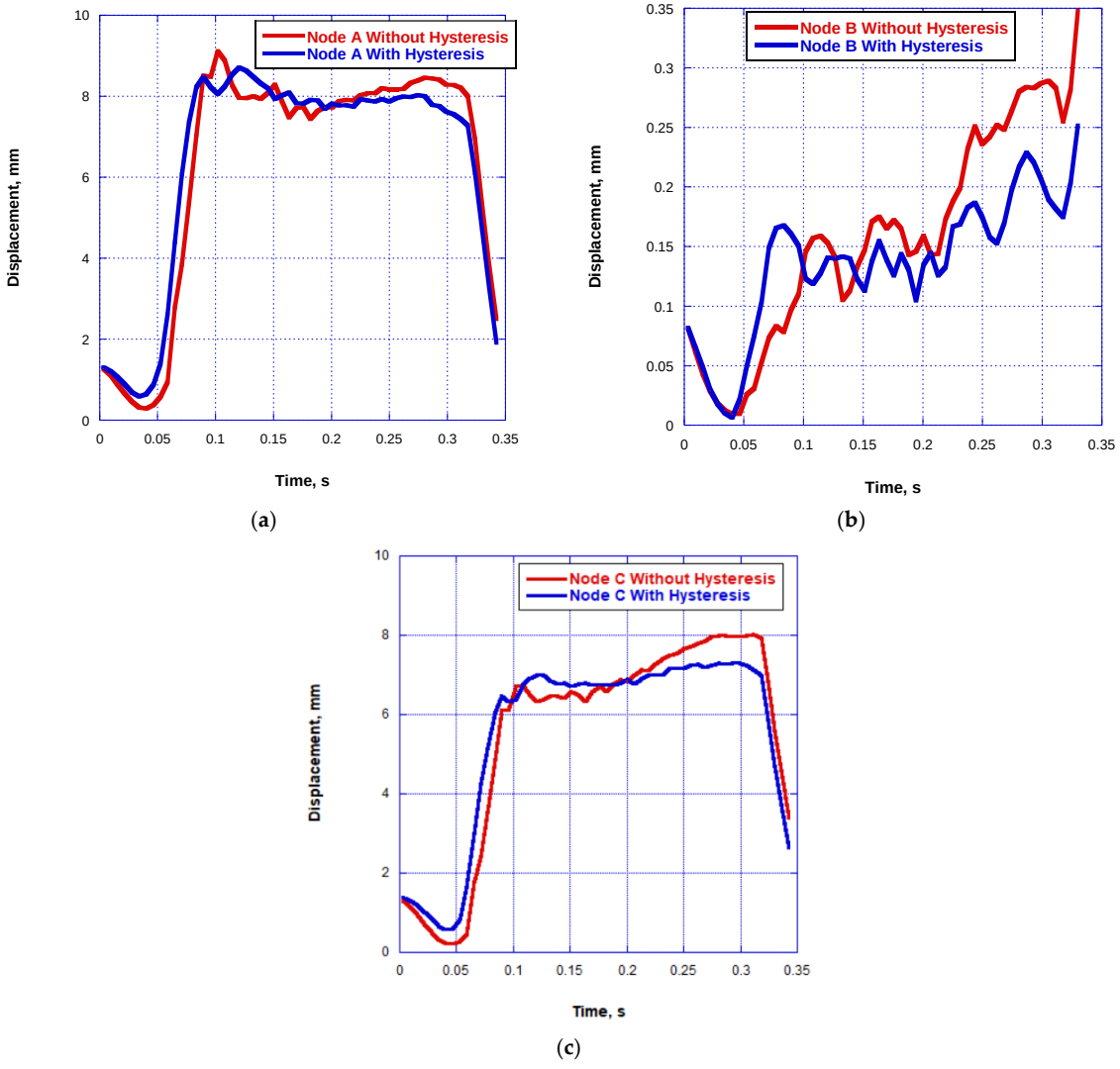

Figure 16. Time-variations of resultant displacement at three points with and without hysteresis. (**a**) Node A, (**b**) Node B, and (**c**) Node C.

4. Conclusions

Explicit dynamic finite element analysis of the artificial polymeric heart valve was conducted by introducing the hyperelastic model with hysteresis. The opening and closing states of the tri-leaflets of the valve during the full cardiac cycle were successfully simulated using this valve model. The hysteresis model affected the deformation behavior dramatically. Especially, the unusual full close form of the pure hyperelastic model with the waved lines was adjusted to the standard straight lines by introducing the hysteresis model. It is thus concluded that the hysteresis model must be introduced into the dynamic analysis of the artificial polymeric valves in order to obtain more realistic deformation behaviors.

Author Contributions: Conceptualization, S.H.M. and M.T.; methodology, S.H.M.; software, M.T.; validation, S.H.M. and M.T.; formal analysis, S.H.M.; investigation, S.H.M. and M.T.; resources, M.T.; writing original draft preparation, S.H.M.; writing review and editing, S.H.M. and M.T.; supervision, M.T.; project administration, M.T.; All authors have read and agreed to the published version of the manuscript.

Funding: This research was partially supported by JSPS Grants-in-Aid for Scientific Research (B) (No.21H01215).

Institutional Review Board Statement: Not applicable.

Informed Consent Statement: Not applicable.

Conflicts of Interest: The authors declare no conflict of interest.

References

1. Labrosse, M.R.; Beller, C.J.; Robicsek, F.; Thubrikar, M.J. Geometric modeling of functional trileaflet aortic valves: Development and clinical applications. *J. Biomech.* **2006**, *39*, 2665–2672. [CrossRef] [PubMed]
2. Kunzelman, K.S.; Grande, K.J.; David, T.E.; Cochran, R.P.; Verrier, E.D. Aortic root and valve relationships: Impact on surgical repair. *J. Thorac. Cardiovasc. Surg.* **1994**, *107*, 162–170. [CrossRef]
3. Lloyd-Jones, D.; Adams, R.J.; Brown, T.M.; Carnethon, M.; Dai, S.; De Simone, G.; Ferguson, T.B.; Ford, E.; Furie, K.; Gillespie, C.; et al. Executive summary: Heart disease and stroke statistics-2010 update: A report from the american heart association. *Circulation* **2010**, *121*, 46–215. [CrossRef]
4. Turitto, V.T.; Hall, C.L. Mechanical factors affecting hemostasis and thrombosis. *Thromb. Res.* **1998**, *92*, S25–S31. [CrossRef]
5. Yoganathan, A.P.; He, Z.; Jones, S.C. Fluid mechanics of heart valves. *Annu. Rev. Biomed. Eng.* **2004**, *6*, 331–362. [CrossRef] [PubMed]
6. Khan, S.S.; Trento, A.; DeRobertis, M.; Kass, R.M.; Sandhu, M.; Czer, L.S.; Blanche, C.; Raissi, S.; Fontana, G.P.; Cheng, W.; et al. Twenty-year comparison of tissue and mechanical valve replacement. *J. Thorac. Cardiovasc. Surg.* **2001**, *122*, 257–269. [CrossRef]
7. Gharaie, S.H.; Morsi, Y. A novel design of a polymeric aortic valve. *Int. J. Artif. Organs* **2015**, *38*, 259–270. [CrossRef]
8. Ando, M.; Takahashi, Y. Ten-year experience with handmade trileaflet polytetrafluoroethylene valved conduit used for pulmonary reconstruction. *J. Thorac. Cardiovasc. Surg.* **2009**, *137*, 124–131. [CrossRef]
9. Ding, N.; Pacetti, S.D.; Tang, F.W.; Gada, M.; Roorda, W. XIENCE V^{TM} stent design and rationale. *J. Interv. Cardiol.* **2009**, *22*, 18–27. [CrossRef]
10. Rahmani, B.; Tzamtzis, S.; Ghanbari, H.; Burriesci, G.; Seifalian, A.M. Manufacturing and hydrodynamic assessment of a novel aortic valve made of a new nanocomposite polymer. *J. Biomech.* **2012**, *45*, 1205–1211. [CrossRef]
11. Braunwald, N.S.; Cooper, T.; Morrow, A.G. Complete replacement of the mitral valve: Successful clinical application of a flexible polyurethane prosthesis. *J. Thorac. Cardiovasc. Surg.* **1960**, *40*, 1–11. [CrossRef]
12. Nistal, F.; Garcia-Martinez, V.; Arbe, E.; Fernandez, D.; Artinano, E.; Mazorra, F.; Gallo, I. In vivo experimental assessment of polytetrafluoroethylene trileaflet heart valve prosthesis. *J. Thorac. Cardiovasc. Surg.* **1990**, *99*, 1074–1081. [CrossRef]
13. Thomas, V.; Jayabalan, M. A new generation of high flex life polyurethane urea for polymer heart valve—Studies on in vivo biocompatibility and biodurability. *J. Biomed. Mater. Res. A* **2009**, *89*, 192–205. [CrossRef]
14. Kidane, A.G.; Burriesci, G.; Edirisinghe, M.; Ghanbari, H.; Bonhoeffer, P.; Seifalian, A.M. A novel nanocomposite polymer for development of synthetic heart valve leaflets. *Acta Biomater.* **2009**, *5*, 2409–2417. [CrossRef] [PubMed]
15. Pinchuk, L.; Wilson, G.J.; Barry, J.J.; Schoephoerster, R.T.; Parel, J.M.; Kennedy, J.P. Medical applications of poly(styrene-block-isobutylene-block-styrene) ("SIBS"). *Biomaterials* **2008**, *29*, 448–460. [CrossRef]
16. Dempsey, D.K.; Carranza, C.; Chawla, C.P.; Gray, P.; Eoh, J.H.; Cereceres, S.; Cosgriff-Hernandez, E.M. Comparative analysis of in vitro oxidative degradation of poly(carbonate urethanes) for biostability screening. *J. Biomed. Mater. Res. A* **2014**, *102*, 3649–3665. [CrossRef]
17. Nic An Ghaill, N.; Little, E.G. Determination of the mechanical properties of Bionate 80A and Bionate 75D for the stress analysis of cushion form bearings. *Proc. Inst. Mech. Eng. H J. Eng. Med.* **2008**, *222*, 683–694. [CrossRef]

18. Melly, S.K.; Liu, L.; Liu, Y.; Leng, J. A review on material models for isotropic hyperelasticity. *Int. J. Mech. Syst. Dyn.* **2021**, *1*, 71–88. [CrossRef]
19. Mihai, L.A.; Chin, L.; Janmey, P.A.; Goriely, A. A comparison of hyperelastic constitutive models applicable to brain and fat tissues. *J. R. Soc. Interface* **2015**, *12*, 20150486. [CrossRef]
20. Inyang, A.O.; Vaughan, C.L. Functional characteristics and mechanical performance of PCU composites for knee meniscus replacement. *Materials* **2020**, *13*, 1886. [CrossRef]
21. Ogden, R.W.; Roxburgh, D.G. A pseudo-elastic model for the Mullins effect in filled rubber. *Proc. R. Soc. A Math. Phys. Eng. Sci.* **1999**, *455*, 2861–2877. [CrossRef]
22. Carleo, F.; Barbieri, E.; Whear, R.; Busfield, J.J.C. Limitations of viscoelastic constitutive models for carbon-black reinforced rubber in medium dynamic strains and medium strain rates. *Polymers* **2018**, *10*, 988. [CrossRef] [PubMed]
23. Ranga, A.; Mongrain, R.; Biadilah, Y.; Cartier, R.; Mcgill, M. A Compliant dynamic FEA Model of the aortic valve. In Proceedings of the 12th IFToMM World Congress, Besancon, France, 18–21 June 2007.
24. Bialas, O.; Zmudzki, J. FEA of displacements and stresses of aortic heart valve leaflets during the opening phase. *J. Achiev. Mater. Manuf. Eng.* **2019**, *92*, 29–35. [CrossRef]